Nonintrusive Parameter Identification of IoT-Embedded Isotropic PMSM Drives

Elia Brescia, Paolo Roberto Massenio, Mauro Di Nardo, *Member, IEEE*, Giuseppe Leonardo Cascella, *Member, IEEE*, Chris Gerada, *Senior Member, IEEE*, and Francesco Cupertino, *Senior Member, IEEE*

***Abstract*— This article proposes a nonintrusive parameter identification procedure suitable for Internet-of-Things (IoT)-embedded isotropic permanent magnet synchronous machines (PMSMs). The method is designed for scenarios where only measurements collected without additional sensors, dedicated tests, or signal injection from in-service off-the-shelves motor drives are available. After automatic detection of the steady-state operating conditions (OCs) defined by the triplet current–speed–temperature, the rotor flux linkage, the stator resistance, the inductance, and the inverter distorted voltage term are estimated using two operating points. Particular emphasis is placed in defining the criteria of selecting these two optimal OCs to minimize the estimation errors. The latter are due to the inevitable difference between the parameters in different operating points. As a vessel to investigate the effectiveness of the proposed parameter identification, experimental and simulation tests carried out on a high-speed PMSM drive have been used for validation purpose. The proposed method is also compared with the existing methods from the literature to demonstrate its superiority in the considered scenario.**

***Index Terms*— Actuation delay compensation, inverter nonlinearity, parameter identification, permanent magnet, rank deficiency, synchronous machines.**

I. Introduction

RECENTLY, the integration of electrical drives with edge and cloud computing systems is becoming more and more popular for condition monitoring, fault diagnosis, and predictive maintenance [1], [2]. In this context, data-driven and machine-learning-based algorithms are the most adopted, while model-based (MB) approaches have not received much attention [3]. However, MB strategies may offer additional advantages if paired with the data-driven algorithms. A consolidated strategy is to execute an analytical digital twin in parallel to the real motor with the same measured inputs while comparing their outputs. The residual signals can be exploited to detect faults in the system using a residual evaluator.

To implement mathematical models of motors, the parameter identification is essential. Moreover, the knowledge of the parameters allows itself for a straightforward fault diagnosis if the model parameters have a one-to-one mapping with the physical coefficients [4]. For instance, the estimation of rotor magnet flux of permanent magnet synchronous machines (PMSMs) can be adopted to detect magnet faults [5], while the interturn short-circuit can abruptly change both the dq-axis inductance and winding resistance [6].

In this study, the problem of parameter identification of Internet-of-Things (IoT)-embedded electrical motor drives is addressed. A schematic of the considered IoT-embedded electrical motor drive is depicted in Fig. 1. The system consists of a standard off-the-shelf motor drive, an IoT device which collects and transmits the data generated by the drive control unit, and a cloud-computing application where the data are stored and processed to accomplish parameter identification. The communication between the drive control unit and the IoT device is enabled by the widespread connectivity properties of modern electric drives. The flexibility and scalability of this architecture allow to easily implement customized parameter identification algorithms for multiple and different in-service motor drives. In the considered setup, the drive control unit shares the data with the IoT device through a unidirectional communication. Therefore, the drive control algorithm is not affected by parameter identification while the estimated parameters can be exploited to implement digital twins, condition monitoring, fault detection, or predictive maintenance procedures.

Thus, this work is based on a realistic scenario where a motor drive provides measurements generated during regular operations. In such a scenario, compared with more conventional contexts such as laboratory tests or electric drive design, additional nonintrusivity and flexibility constraints must be considered to design a suitable parameter identification technique:

1) To simplify the system and reduce costs, additional measurement devices are not allowed;

Manuscript received 13 March 2023; revised 27 May 2023 and 12 June 2023; accepted 14 June 2023. Date of publication 5 July 2023; date of current version 3 October 2023. This work was supported in part by the Project "YGF1OI5—Progetto di Ricerca e Sviluppo di tecnologie sostenibile applicate a prodotti innovativi per la gestione della trazione in campo ferroviario" in collaboration with Tesmec Rail srl. Recommended for publication by Associate Editor Joseph Olorunfemi Ojo. *(Corresponding author: Elia Brescia.)*

Elia Brescia, Paolo Roberto Massenio, Giuseppe Leonardo Cascella, and Francesco Cupertino are with the Department of Electrical and Information Engineering, Politecnico di Bari, 70125 Bari, Italy (e-mail: elia.brescia@poliba.it; paoloroberto.massenio@poliba.it; giuseppeleonardo.cascella@poliba.it; francesco.cupertino@poliba.it).

Mauro Di Nardo and Chris Gerada are with the Power Electronics and Machine Control Group, University of Nottingham, NG7 2GT Nottingham, U.K. (e-mail: mauro.dinardo4@nottingham.ac.uk; chris.gerada@nottingham.ac.uk).

Color versions of one or more figures in this article are available at https://doi.org/10.1109/JESTPE.2023.3292526.

Digital Object Identifier 10.1109/JESTPE.2023.3292526

2) To avoid machine downtimes, ad hoc tests to collect data are not allowed;
3) Since in-service off-the-shelves commercial motor drives are considered, a customized control logic cannot be implemented to inject perturbation signals;
4) The algorithm must be flexible to operate even in case of few available speed/load operating conditions (OCs).

In particular, the parameter identification problem is formulated for PMSMs, which are widely used in the industry [7], electric transportation [8], and renewable energy [9]. The identification of PMSM parameters, such as inductances, rotor flux linkage, and stator resistance has been a subject of a vast literature in the past decades. The numerous parameters' estimation techniques reported in literature are categorized into two main families: offline and online estimation methods.

The offline methods need specific laboratory equipment with the machine usually disconnected from its load or require multiple measurements collected in different motor OCs achieved with ad hoc tests [10]. For instance, in [11], an offline procedure is proposed in which the rotor flux linkage is estimated using line-to-line voltage measurements during a test in which an induction motor is powered to drive the PMSM. Instead, to identify the stator resistance and inductance, an additional single-phase voltage source is connected to the PMSM to collect the required measurements. In [12], no load and load tests on several operating points in the entire torque–speed range are performed to identify the motor parameters. In [13], the measurements are collected under multiple predefined speed and current conditions achieved with ad hoc tests.

Instead, online parameter identification methods are usually implemented on the drive control unit during the motor operation relying on the injection of perturbation signals to overcome the rank-deficiency issue. For instance, in [6], a d-axis current is injected to obtain two steady-state equations required to identify the parameters. In [14], two position offsets are intentionally added into the drive system, and the machine measurements corresponding to the two offsets are recorded before the estimation. In [15], an additional temporary steady-state is designed for the simultaneous estimation of flux, resistance, and dq-axis inductances of a salient-pole PMSM. It is clear that both the approaches are inadequate to be adopted in the scenario considered in this work.

A first work that addresses parameter identification of a PMSM using cloud computing resources was presented in [16]. In this article, an edge/cloud computing architecture based on Amazon Web Services (AWS) is arranged to collect motor measurements generated without signal injection or ad hoc tests and to perform a parameter identification based on three Adaline neural networks. However, this work lacks validation through experimental data collected from a real motor. Moreover, this work is based on simplifying assumptions, such as the availability of the measured voltages and the absence of parameter variations.

In this article, a novel parameter identification method for isotropic PMSM drives controlled with the zero d-axis current is proposed. Note that this is the most widespread typology among PMSM drives and can also be considered the most investigated for parameter identification [6], [11], [14], [17], [18], [19], [20], [21], [22]. In particular, to satisfy the nonintrusivity constraints imposed by the considered scenario, the motor parameters are estimated using only measurements commonly available in commercial PMSM drives (such as rotor position, currents, voltage references, and motor temperature) collected during the regular operation of the motor without injection of perturbation signals or ad hoc tests. Moreover, to make the method more flexible and to extend its applicability in contexts where few load/speed OCs are available, the identification algorithm is designed to operate only with two steady-states.

Since the motor parameters may vary among the PMSM steady-states due to temperature and frequency changes, a theoretical analysis is presented to determine the estimation errors caused by parameter variations. Therefore, according to this analysis, when only two OCs are available, the proposed identification method evaluates the feasibility of the estimations. Instead, when more than two OCs are available, an optimization algorithm selects the two OCs used to identify the parameters which minimize the estimation errors.

Note that since the proposed method relies on the voltage references instead of the measured voltages, the estimation accuracy can be further endangered [22]. The mismatch between these two quantities is caused by actuation delays and inverter nonlinearity, i.e., voltage drops on power devices and dead-time effect [23]. The inverter distortion does not affect the estimation of the q-axis inductance when the d-axis current is controlled to zero [23], while the actuation delay affects all the parameters. In particular, the actuation delay causes a voltage distortion which increases when the ratio between electrical rotor speed and control sampling frequency increases. As a consequence, identification procedures relying on voltage references are usually carried out at low speeds where this effect is negligible [6], [20]. In this article, both inverter nonlinearity and actuation delay are considered and compensated to increase the accuracy also in medium- and high-frequency applications.

The rest of this article is organized as follows. Section II summarizes the PMSM model with actuation delays and inverter nonlinearity, while the proposed identification algorithm is detailed in Section III. The validation methodology is discussed in Section IV while the simulation results and the experimental validation are reported and commented in Sections V and VI, respectively.

II. Formulation of the Parameter Identification Problem

A stationary discrete-time mathematical model largely adopted for the design of online identification algorithms of isotropic PMSM with d-axis current, i_d, equal to zero, is based on the following equations [6], [22], [24]:

$$u_d^*(k) = -L\omega(k)\, i_q(k) - D_d(k)\, V_{\text{dead}} \tag{1a}$$

$$u_q^*(k) = Ri_q(k) + \psi_m\omega(k) - D_q(k)\, V_{\text{dead}} \tag{1b}$$

where k denotes the kth sample, u_{dq}^* are the voltage references, i_q is the q-axis current, ω is the electrical rotor speed, V_{dead} is

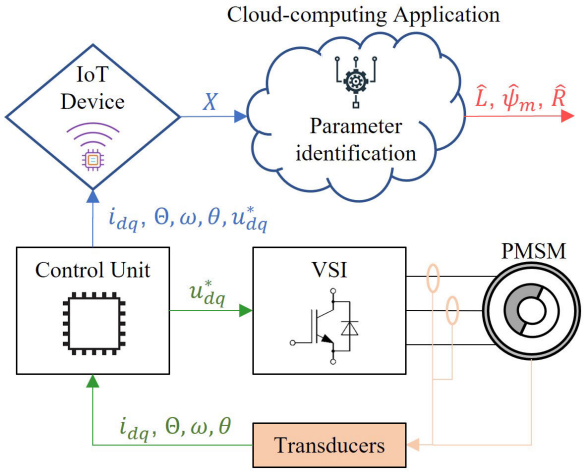

Fig. 1. IoT-embedded drive schematic.

the distorted voltage, D_d and D_q are the distorted coefficients as in [5], and L, R, and ψ_m are the stator inductance, the stator resistance, and the rotor flux linkage, respectively. The sampling time of (1) is T_s. This model is based on the common assumptions that the dq-axis inductances are equal and iron losses are negligible in isotropic PMSMs [21], [23].

Since temperature measurements are usually available in commercial PMSM drives [25], the model can be improved by introducing the temperature correction of R

$$u^*_d(k) = -L\omega(k)\, i_q(k) - D_d(k)\, V_{\text{dead}} \tag{2a}$$

$$u^*_q(k) = (1 + \alpha_0 \Delta\Theta(k))\, R'_{\text{ac}} i_q(k) + \psi_m \omega(k) - D_q(k)\, V_{\text{dead}} \tag{2b}$$

where $\Delta\Theta = \Theta - 20\ ^\circ\text{C}$, with Θ motor temperature, α_0 is the copper temperature coefficient, and R'_{ac} is the ac stator resistance factor. Note that this PMSM model has four unknown parameters to be identified, i.e., L, R'_{ac}, ψ_m, and V_{dead}, while its rank is at most 2. Therefore, in principle, only two PMSM steady-states are required to estimate the parameters.

To increase the estimation accuracy, more complex models are considered in offline estimation methods. For instance, in [26], a model which also includes iron losses and self- and cross-saturation is considered. The study presented in [27] shows that the ac stator resistance is actually a function of temperature and frequency by means of additional coefficients and parameters to be identified. Obviously, the increased complexity of the model results in more parameters to be identified and in additional PMSM OCs required to solve the parameter identification problem. However, in the considered scenario, the PMSM OCs cannot be arbitrarily obtained with ad hoc tests since only measurements collected during the regular operation of the motor can be exploited. Therefore, in this study, the model (2) is chosen as it is simple and flexible to operate even in case of PMSMs working in few different conditions.

The accuracy of (2) is further improved by compensating the delay between the actual voltages and the reference voltages, which is equal to $1.5T_s$ in the PMSM

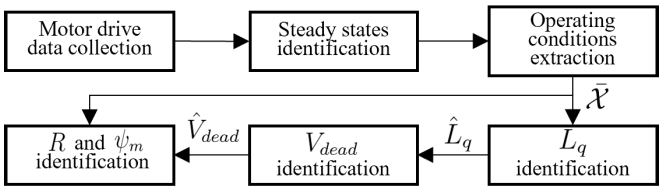

Fig. 2. Main steps of the proposed identification method.

digital control system [28]

$$\tilde{u}_{dq}(k) = \begin{bmatrix} \cos(\Delta\theta(k)) & \sin(\Delta\theta(k)) \\ -\sin(\Delta\theta(k)) & \cos(\Delta\theta(k)) \end{bmatrix} u^*_{dq}(k-1) \tag{3}$$

where $\Delta\theta$ is the rotor electrical angular displacement due to the digital delay. By assuming constant speed during this short period, $\Delta\theta$ is expressed as

$$\Delta\theta(k) = \frac{3}{2}(\theta(k) - \theta(k-1)) \tag{4}$$

where θ is the rotor electrical position. Note that since $\Delta\theta(k) \approx (3/2)\omega(k)T_s$, the voltage distortion caused by the digital delay is expected to increase with the speed of the motor. By considering (3), the definitive model adopted in this study is

$$\tilde{u}_d(k) = -L\omega(k)\, i_q(k) - D_d(k)\, V_{\text{dead}} \tag{5a}$$

$$\tilde{u}_q(k) = (1 + \alpha_0 \Delta\Theta(k))\, R'_{\text{ac}} i_q(k) + \psi_m \omega(k) - D_q(k)\, V_{\text{dead}}. \tag{5b}$$

III. Proposed Parameter Identification Method

Fig. 2 shows the high-level procedure of the proposed parameter identification detailed in Sections III-A–III-D. The identification of the electromagnetic steady-states defined by a given speed and current values is outlined in Section III-A along with extraction of the OCs defined by a certain speed, current, and stator temperature. Section III-B describes the identification of L and V_{dead}, while Section III-C details the estimations of R'_{ac} and ψ_m. The selection of the best OCs used to estimate R'_{ac} and ψ_m is described in Section III-D.

A. Extraction of the OCs

The formulated parameter identification problem is based on the stationary model of the PMSM. Therefore, the automated detection of the motor steady-states is required. In this study, a steady-state is detected when the recorded current and speed show a constant behavior according to the R-statistic paradigm [16]. Instead, the PMSM transient states due to speed and load variations are automatically excluded from the collected measurements. Let N_s be the number of detected steady-states. Then, X_i, with $i = 1, \ldots, N_s$, denotes the set containing the data of the ith steady-state, as follows:

$$X_i = \{\omega_i(1), \ldots, \omega_i(N_i), i_{q_i}(1), \ldots, i_{q_i}(N_i), \tilde{u}_{dq_i}(1), \ldots, \tilde{u}_{dq_i}(N_i), D_{d_i}(1), \ldots, D_{d_i}(N_i), D_{q_i}(1), \ldots, D_{q_i}(N_i), \Theta_i(1), \ldots, \Theta_i(N_i)\} \tag{6}$$

where N_i is the number of samples within the ith steady-state, and Θ_i represents the motor temperature. Note that

in (6) speed and current are at the steady-state while the motor temperature may vary. Since both R and ψ_m depend on the temperature, it is congruous to consider different OCs within each electromagnetic steady-state according to thermal transients. Therefore, in each X_i, a set of OCs are extracted as follows.

First, the raw data in each X_i are properly sliced. Let $k_{i,h_s}, k_{i,h_e} \in \{1,\dots,N_i\}$, with $k_{i,h_e} > k_{i,h_s}$, be the start and end samples of the hth data slice, respectively. k_{i,h_s} and k_{i,h_e} are such that $|\Theta_i(k_{i,h_s}) - \Theta_i(k_{i,h_e})| \approx \Delta\Theta_r$. That is, each slice is a subset of the data in X_i corresponding to a temperature range that is approximately $\Delta\Theta_r$. Then, each hth slice in X_i is represented by the t-uple $(\bar{\omega}_{i_j}, \bar{i}_{q_{i_j}}, \bar{\tilde{u}}_{dq_{i_j}}, \bar{D}_{d_{i_j}}, \bar{D}_{q_{i_j}}, \bar{\Theta}_{i_j})$ obtained by averaging each variable within the slice.

Now let $\bar{\mathcal{X}} = \{\bar{X}_1,\dots,\bar{X}_{N_{\rm OC}}\}$ be the set of the OCs extracted from all X_i sets. Each OC is represented by $\bar{X}_j = \begin{bmatrix}\bar{\omega}_j & \bar{i}_{q_j} & \bar{\tilde{u}}_{dq_j} & \bar{D}_{d_j} & \bar{D}_{q_j} & \bar{\Theta}_j\end{bmatrix}$, $j = 1,\dots,N_{\rm OC}$. For each X_i, the t-uples corresponding to the first and last data slices constitute the first two OCs extracted. Then, other OCs are extracted at a temperature step of $\Delta\Theta_s$. That is, if there exist two data slices, indexed by $h1$ and $h2$, such that $|\bar{\Theta}_{1_{h1}} - \bar{\Theta}_{1_{h2}}| \approx \Delta\Theta_s$, the corresponding t-uples are added as OCs in $\bar{\mathcal{X}}$. Clearly, $\Delta\Theta_s$ is selected greater than $\Delta\Theta_r$.

To sum up, the extraction procedure starts from the raw data of each identified steady-state, X_i, to produce the set of OCs, $\bar{\mathcal{X}}$, to be used in parameter identification. Two or more OCs in $\bar{\mathcal{X}}$ may share the same steady-state values of speed and current but feature different temperatures (with a step of $\Delta\Theta_s$ degrees).

B. L and V_{dead} Identification

After the OCs have been extracted, the inductance in each OC, L_j, can be identified using (5a)

$$\hat{L}_j = \frac{-\bar{\tilde{u}}_{d_j}}{\bar{\omega}_j \bar{i}_{q_j}} \tag{7}$$

where $D_d V_{\rm dead}$ is neglected as it is a periodic function of period $(2\pi)/(6\bar{\omega}_j)$ with zero-mean when $i_d = 0$ [20]. This is a simple solution whose main novelty relies on to use of the d-axis delay-compensated voltage, which ensures higher accuracy compared with conventional approaches based on the use of the d-axis voltage reference. It is also worth noting that since only one OC is required to estimate L, the variation in this parameter due to saturation effects among the collected OCs can be effectively tracked.

While the voltage source inverter (VSI) nonlinearity does not affect the estimation of L, it affects the estimation of ψ_m and $R'_{\rm ac}$ as the term $D_q V_{\rm dead}$ in (5b) has a nonzero mean value. Therefore, it is necessary to estimate $V_{\rm dead}$ to ensure the accuracy of the estimation of ψ_m and $R'_{\rm ac}$. The identification of $V_{{\rm dead}_j}$ can be addressed by solving the following minimization problem for each OC, derived from (5a):

$$\min_{\hat{V}_{{\rm dead}_j}} \sum_{k=k_{s_{i,h}}}^{k_{e_{i,h}}} \left(\left(D_{d_i}(k)\,\hat{V}_{{\rm dead}_j} + \tilde{u}_{d_i}(k) + \hat{L}_j \omega_i(k)\, i_{q_i}(k)\right)\right)^2 \tag{8}$$

where i and h denote the ith steady-state and the hth slice corresponding to the jth OC in $\bar{\mathcal{X}}$, respectively. The effectiveness of the search depends on the availability of samples in a period of $D_d V_{\rm dead}$, which decreases as the motor speed increases since the sample time T_s is fixed. Note that also to identify $V_{\rm dead}$, only one OC is required.

C. R'_{ac} and ψ_m Identification

To obtain a full-rank identification problem for $R'_{\rm ac}$ and ψ_m, two different OCs, $\alpha, \beta \in \{1,\dots,N_{\rm OC}\}$, are used. In this way, a set of two equations are derived from (5b)

$$\begin{bmatrix}\bar{\tilde{u}}_{q_\alpha} + \bar{D}_{q_\alpha}\hat{V}_{{\rm dead}_\alpha} \\ \bar{\tilde{u}}_{q_\beta} + \bar{D}_{q_\beta}\hat{V}_{{\rm dead}_\beta}\end{bmatrix} = \begin{bmatrix}\left(1+\alpha_0\Delta\bar{\Theta}_\alpha\right)\bar{i}_{q_\alpha} & \bar{\omega}_\alpha \\ \left(1+\alpha_0\Delta\bar{\Theta}_\beta\right)\bar{i}_{q_\beta} & \bar{\omega}_\beta\end{bmatrix}\begin{bmatrix}\hat{R}'_{\rm ac} \\ \hat{\psi}_m\end{bmatrix} \tag{9}$$

where $\hat{R}'_{\rm ac}$ and $\hat{\psi}_m$ are, respectively, the estimated stator resistance and rotor flux linkage. To obtain two linearly independent equations, the OCs α and β must be selected such that

$$r = \frac{\left(1+\alpha_0\Delta\bar{\Theta}_\alpha\right)\bar{i}_{q_\alpha}\bar{\omega}_\beta}{\left(1+\alpha_0\Delta\bar{\Theta}_\beta\right)\bar{i}_{q_\beta}\bar{\omega}_\alpha} \neq 1. \tag{10}$$

If (10) is satisfied, $\hat{R}'_{\rm ac}$ and $\hat{\psi}_m$ are obtained as

$$\hat{R}'_{\rm ac} = \frac{-\frac{\bar{\omega}_\beta}{\bar{\omega}_\alpha}\left(\bar{\tilde{u}}_{q_\alpha} + \bar{D}_{q_\alpha}\hat{V}_{{\rm dead}_\alpha}\right) + \bar{\tilde{u}}_{q_\beta} + \bar{D}_{q_\beta}\hat{V}_{{\rm dead}_\beta}}{\bar{i}'_{q_\beta}(1-r)} \tag{11a}$$

$$\hat{\psi}_m = \frac{\bar{\tilde{u}}_{q_\alpha} + \bar{D}_{q_\alpha}\hat{V}_{{\rm dead}_\alpha} - \left(\bar{\tilde{u}}_{q_\beta} + \bar{D}_{q_\beta}\hat{V}_{{\rm dead}_\beta}\right)\frac{\bar{i}'_{q_\alpha}}{\bar{i}'_{q_\beta}}}{\bar{\omega}_\alpha(1-r)} \tag{11b}$$

where $\bar{i}'_{q_\iota} = (1+\alpha_0\Delta\bar{\Theta}_\iota)\bar{i}_{q_\iota}$, with $\iota = \alpha, \beta$.

Considering the parameter dependence on the OCs and the presence of voltage errors due to imperfect digital delay and VSI nonlinearity compensation and measurement errors of speed and currents, (5b) can be rewritten as follows:

$$\bar{\tilde{u}}_{q_\alpha} + \bar{D}_{q_\alpha}\hat{V}_{{\rm dead}_\alpha} = R'_{{\rm ac}_\alpha}\bar{i}'_{q_\alpha} + \psi_{m_\alpha}\bar{\omega}_\alpha + \varepsilon_{u_{q\alpha}} \tag{12a}$$

$$\bar{\tilde{u}}_{q_\beta} + \bar{D}_{q\beta}\hat{V}_{{\rm dead}_\beta} = R'_{{\rm ac}_\beta}\bar{i}'_{q_\beta} + \psi_{m_\beta}\bar{\omega}_\beta + \varepsilon_{u_{q\beta}} \tag{12b}$$

where $R'_{{\rm ac}_\alpha}$, $R'_{{\rm ac}_\beta}$, ψ_{m_α}, ψ_{m_β}, $\varepsilon_{u_{q\alpha}}$, and $\varepsilon_{u_{q\beta}}$ are the unknown actual values of the stator resistance, rotor flux linkage, and voltage errors in the OCs α and β, respectively. By substituting (12a) and (12b) in (11b), the following equivalent expressions of $\hat{\psi}_m$ are obtained:

$$\begin{aligned}\hat{\psi}_m &= \psi_{m_\alpha} + \varepsilon_{\psi_{m\alpha}} + \varepsilon_{\psi_M} \\ \hat{\psi}_m &= \psi_{m_\beta} + \varepsilon_{\psi_{m\beta}} + \varepsilon_{\psi_M}\end{aligned} \tag{13}$$

where

$$\begin{aligned}\varepsilon_{\psi_{m\alpha}} &= \frac{\left(\psi_{m_\alpha} - \psi_{m_\beta}\right)r}{1-r} + \frac{\left(R'_{{\rm ac}_\alpha} - R'_{{\rm ac}_\beta}\right)\frac{\bar{i}'_{q_\alpha}}{\bar{\omega}_\alpha}}{1-r} \\ \varepsilon_{\psi_{m\beta}} &= \frac{\left(\psi_{m_\alpha} - \psi_{m_\beta}\right)}{1-r} + \frac{\left(R'_{{\rm ac}_\alpha} - R'_{{\rm ac}_\beta}\right)\frac{\bar{i}'_{q_\alpha}}{\bar{\omega}_\alpha}}{1-r} \\ \varepsilon_{\psi_M} &= \frac{\varepsilon_{u_{q\alpha}} - \varepsilon_{u_{q\beta}}\frac{\bar{i}'_{q_\alpha}}{\bar{i}'_{q_\beta}}}{\bar{\omega}_\alpha(1-r)}.\end{aligned} \tag{14}$$

With the same approach, by substituting (12a) and (12b) into (11a), the following expressions of $\hat{R}'_{\mathrm{ac}}$ are obtained:

$$\begin{aligned}\hat{R}'_{\mathrm{ac}_\alpha} &= R'_{\mathrm{ac}_\alpha} + \varepsilon_{R_\alpha} + \varepsilon_{R_M}\\ \hat{R}'_{\mathrm{ac}_\beta} &= R'_{\mathrm{ac}_\beta} + \varepsilon_{R_\beta} + \varepsilon_{R_M}\end{aligned} \tag{15}$$

where

$$\begin{aligned}\varepsilon_{R_\alpha} &= \frac{R'_{\mathrm{ac}_\beta} - R'_{\mathrm{ac}_\alpha}}{1-r} + \frac{\left(\psi_{m_\beta} - \psi_{m_\alpha}\right)\frac{\bar{\omega}_\beta}{\bar{i}'_{q_\beta}}}{1-r}\\ \varepsilon_{R_\beta} &= \frac{\left(R'_{\mathrm{ac}_\beta} - R'_{\mathrm{ac}_\alpha}\right)r}{1-r} + \frac{\left(\psi_{m_\beta} - \psi_{m_\alpha}\right)\frac{\bar{\omega}_\beta}{\bar{i}'_{q_\beta}}}{1-r}\\ \varepsilon_{R_M} &= \frac{\varepsilon_{u_{q\beta}} - \varepsilon_{u_{q\alpha}}\frac{\bar{\omega}_\beta}{\bar{\omega}_\alpha}}{\bar{i}'_{q_\beta}(1-r)}.\end{aligned} \tag{16}$$

Note that $\hat{R}'_{\mathrm{ac}}$ and $\hat{\psi}_m$ are given by the actual values in the two OCs α or β, i.e., ψ_{m_α}, ψ_{m_β}, and R'_{ac_α}, R'_{ac_β}, plus two components of the estimation error. The first component, i.e., $\varepsilon_{\psi_{m\alpha}}$ and $\varepsilon_{\psi_{m\beta}}$ in (13), and ε_{R_α} and ε_{R_β} in (15), is caused by the mismatch of the two parameters in the two OCs. The second component, i.e., ε_{ψ_M} in (13), and ε_{R_M} in (15), is caused by the voltage errors.

D. Minimization of the Estimation Errors

The estimation errors depend on the speed, temperature, and q-axis current of both OCs α and β [see (14) and (16)]. Therefore, the majorant of the estimation error can be minimized by properly selecting these two OCs. With reference to the estimation of R'_{ac} in the αth OC, the majorant of the estimation error, i.e., $\tilde{\varepsilon}_{R_\alpha\mathrm{tot}}$, is derived from (16)

$$\tilde{\varepsilon}_{R_\alpha\mathrm{tot}} = \tilde{\varepsilon}_{R_\alpha} + \tilde{\varepsilon}_{R_M} \tag{17}$$

with

$$\begin{aligned}\tilde{\varepsilon}_{R_\alpha} &= \left|\frac{\tilde{R}'_{\mathrm{ac}_\beta} - \tilde{R}'_{\mathrm{ac}_\alpha}}{1-r}\right| + \left|\frac{\left(\tilde{\psi}_{m_\beta} - \tilde{\psi}_{m_\alpha}\right)\frac{\bar{\omega}_\beta}{\bar{i}'_{q_\beta}}}{1-r}\right|\\ \tilde{\varepsilon}_{R_M} &= \frac{\left|\tilde{\varepsilon}_{u_q}\right| + \left|\tilde{\varepsilon}_{u_q}\frac{\bar{\omega}_\beta}{\bar{\omega}_\alpha}\right|}{\left|\bar{i}'_{q_\beta}(1-r)\right|}\end{aligned} \tag{18}$$

where $\tilde{R}'_{\mathrm{ac}_\iota}$ and $\tilde{\psi}_{m_\iota}$ are rough estimations of R'_{ac_ι} and ψ_{m_ι}, respectively, with $\iota = \alpha, \beta$. $\tilde{\varepsilon}_{u_q}$ is the supposed voltage error.

The rough estimations are computed using only temperature and speed data, i.e., considering the following [27], [29], [30]:

$$\begin{aligned}\tilde{R}'_{\mathrm{ac}_\iota} &= \tilde{R}_{\mathrm{dc}_0}\frac{\left(1+\tilde{\beta}_0\left(\frac{\bar{\omega}_\iota}{2\pi}\right)^2\right)-1}{\left(1+\alpha_0\left(\bar{\Theta}_\iota - 20\right)\right)^{\tilde{\gamma}+1}} + \tilde{R}_{\mathrm{dc}_0}\\ \tilde{\psi}_{m_\iota} &= \tilde{\psi}_0\left(1+\tilde{\alpha}_{\mathrm{PM0}}\left(\bar{\Theta}_\iota - 20\right)\right)\end{aligned} \tag{19}$$

where $\tilde{R}_{\mathrm{dc}_0}$ and $\tilde{\psi}_0$ are rough estimations of R and ψ_m at zero speed and 20 °C, $\tilde{\beta}_0$ is the supposed quadratic frequency coefficient, $\tilde{\gamma}$ is the supposed temperature coefficient of the ac resistance, and $\tilde{\alpha}_{\mathrm{PM0}}$ is the supposed PMs' temperature coefficient. The use of precautionary values for $\tilde{\varepsilon}_{u_q}$, $\tilde{\beta}_0$, $\tilde{\gamma}$, and $\tilde{\alpha}_{\mathrm{PM0}}$ ensures that

$$\tilde{\varepsilon}_{R_\alpha\mathrm{tot}} > \varepsilon_{R_\alpha} + \varepsilon_{R_M}. \tag{20}$$

In particular, for the choice of $\tilde{\beta}_0$, a conservative assumption is that the ac resistance at rated speed is at most ten times the dc resistance. According to this assumption, it can be assumed that

$$\left(1+\beta_0\left(\frac{\omega_r}{2\pi}\right)^2\right) = 10 \tag{21}$$

where ω_r is the electrical rated speed. Therefore, the following formula is adopted to calculate $\tilde{\beta}_0$:

$$\tilde{\beta}_0 = \frac{9}{\left(\frac{\omega_r}{2\pi}\right)^2}. \tag{22}$$

Furthermore, considering that commonly γ is in the range [0 1], it is precautionary set $\tilde{\gamma} = 0$ [27], [31]. Finally, for the choice of $\tilde{\alpha}_{\mathrm{PM0}}$, it should be considered that for PMs, the actual temperature coefficient α_{PM0} is in the range $[-0.2 - 0.02]\%/°\mathrm{C}$. Therefore, in this study, it is chosen $\tilde{\alpha}_{\mathrm{PM0}} = -0.1\%/°\mathrm{C}$.

To obtain $\tilde{R}_{\mathrm{dc}_0}$, the OCs α and β are selected as follows:

$$\begin{aligned}[\alpha,\beta] = \underset{\substack{i\in S_R\\ j=1,\ldots,N_{\mathrm{OC}}\\ i\neq j}}{\operatorname{argmin}} & \frac{\left|\tilde{\varepsilon}_{u_q}\right| + \left|\tilde{\varepsilon}_{u_q}\frac{\bar{\omega}_j}{\bar{\omega}_i}\right|}{\left|\bar{i}'_{q_j}\left(1-\frac{\bar{i}'_{q_i}\bar{\omega}_j}{\bar{i}'_{q_j}\bar{\omega}_i}\right)\right|}\\ \text{s.t.} & \left|\frac{\bar{i}'_{q_i}\bar{\omega}_j}{\bar{i}'_{q_j}\bar{\omega}_i}\right| > r_{\mathrm{lim}}\end{aligned} \tag{23}$$

where r_{lim} is a positive tuning parameter that ensures to reduce estimation errors [see (16)], and S_R is a set of OCs determined as follows:

$$\begin{aligned}S_R &= \left\{i = 1,\ldots,N_{\mathrm{OC}} : \frac{\left|\bar{\omega}_i^2 - \bar{\omega}_w^2\right|}{\bar{\omega}_w^2} < f_{\mathrm{lim}}\right\}\\ [w] &= \underset{t=1,\ldots,N_{\mathrm{OC}}}{\operatorname{argmin}} \left|\bar{\omega}_t\right|\end{aligned} \tag{24}$$

in which f_{lim} is a positive dimensionless tuning coefficient.

Problem (23) is built given that $\tilde{R}_{\mathrm{dc}_0}$ is computed by correcting the resistance estimation in α, i.e., $\hat{R}'_{\mathrm{ac}_\alpha}$. Thus, it is convenient to find OC α such that $\hat{R}'_{\mathrm{ac}_\alpha}$ is close to $\tilde{R}_{\mathrm{dc}_0}$, i.e., $\bar{\Theta}_\alpha$ near 20 °C and $\bar{\omega}_\alpha$ near zero. While the temperature correction is more reliable as the actual temperature coefficient of the ac resistance γ varies little around the value $\tilde{\gamma} = 0.5$ [27], this is not true for the frequency correction as the actual frequency coefficient β_0 largely depends on the machine. Therefore, to not add conservativeness to (23), it is only considered that $\bar{\omega}_\alpha$ is minimized [see (24)]. To increase the accuracy of $\tilde{R}_{\mathrm{dc}_0}$, also the estimation errors $\tilde{\varepsilon}_{R_\alpha}$ and $\tilde{\varepsilon}_{R_M}$ have to be minimized. $\tilde{\varepsilon}_{R_\alpha}$ cannot be explicitly minimized as the parameter estimations are not known. However, as in (18), $\tilde{\varepsilon}_{R_\alpha}$ can be made small by selecting two OCs α and β which make $|1-r|$ big [second constraint in (23)]. Instead, $\tilde{\varepsilon}_{R_M}$ is minimized by considering it as objective function. Given α

and β from (23), $\hat{R}'_{\mathrm{ac}_\alpha}$ is computed according to (11a). Finally, a temperature and frequency correction provides $\tilde{R}_{\mathrm{dc}_0}$

$$\tilde{R}_{\mathrm{dc}_0} = \hat{R}'_{\mathrm{ac}_\alpha} \frac{\left(1+\alpha_0\left(\bar{\Theta}_\alpha - 20\right)\right)^{\tilde{\gamma}+1}}{\tilde{\beta}_0\left(\frac{\bar{\omega}_\alpha}{2\pi}\right)^2 + \left(1+\alpha_0\left(\bar{\Theta}_\alpha - 20\right)\right)^{\tilde{\gamma}+1}}. \quad (25)$$

With similar considerations, to obtain $\tilde{\psi}_0$, the OCs α and β are selected as follows:

$$[\alpha,\beta] = \underset{\substack{i=1,\dots,N_{\mathrm{OC}} \\ j\in S_\psi \\ i\neq j}}{\operatorname{argmin}} \frac{\left|\tilde{\varepsilon}_{u_q}\right| + \left|\tilde{\varepsilon}_{u_q}\frac{\bar{i}'_{q_i}}{\bar{i}'_{q_j}}\right|}{\left|\bar{\omega}_i\left(1-\frac{\bar{i}'_{q_i}\bar{\omega}_j}{\bar{i}'_{q_j}\bar{\omega}_i}\right)\right|}$$
$$\text{s.t.} \left|\frac{\bar{i}'_{q_i}\bar{\omega}_j}{\bar{i}'_{q_j}\bar{\omega}_i}\right| > r_{\mathrm{lim}} \quad (26)$$

where S_ψ is a set of OCs determined as follows:

$$S_\psi = \left\{j = 1,\dots,N_{\mathrm{OC}} : \left|\bar{\Theta}_j - \bar{\Theta}_w\right| < \Theta_{\mathrm{lim}}\right\}$$
$$[w] = \underset{t=1,\dots,N_{\mathrm{OC}}}{\operatorname{argmin}} \left|\bar{\Theta}_t\right| \quad (27)$$

where Θ_{lim} is a positive tuning parameter. Given α and β from (26), the estimation of ψ_m in OC β, i.e., $\hat{\psi}_{m_\beta}$, is computed according to (11b). Finally, a temperature correction provides $\tilde{\psi}_0$

$$\tilde{\psi}_0 = \frac{\hat{\psi}_{m_\beta}}{1+\tilde{\alpha}_{\mathrm{PM0}}\left(\bar{\Theta}_\beta - 20\right)}. \quad (28)$$

The majorant of the estimation error of ψ_m in the βth OC, $\tilde{\varepsilon}_{\psi_\beta \mathrm{tot}}$, can be similarly computed with the procedure outlined for R'_{ac}. Once the rough estimations are obtained, the error majorants can be explicitly computed and minimized. For each OC $\alpha \in \{1,\dots,N_{\mathrm{OC}}\}$ in which $\hat{R}'_{\mathrm{ac}_\alpha}$ has to be determined, called main OC (MOC), an OC β, called auxiliary OC (AOC), is chosen to minimize $\tilde{\varepsilon}_{R_\alpha \mathrm{tot}}$, i.e.,

$$\beta = \underset{\substack{i=1,\dots,N_{\mathrm{OC}} \\ i\neq j}}{\operatorname{argmin}} \tilde{\varepsilon}_{R_\alpha \mathrm{tot}}$$
$$\text{s.t. } r < \varepsilon_{r_1} \text{ or } r > \varepsilon_{r_2}, \quad \text{and } \tilde{\varepsilon}_{R_j \mathrm{tot}} < x_R \tilde{R}_\alpha \quad (29)$$

where $\varepsilon_{r_1} < 1$ and $\varepsilon_{r_2} > 1$ are two tunable thresholds which avoid choosing r close to 1, while x_R is a tunable value between 0 and 1. Note that an estimation in an OC α can be rejected if there does not exist an AOC so that $\tilde{\varepsilon}_{R_\alpha \mathrm{tot}}$ is less than a given fraction of $\tilde{R}'_{\mathrm{ac}_\alpha}$, i.e., $x_R \tilde{R}'_{\mathrm{ac}_\alpha}$. Once the AOC is found, α and β are set and the estimation is obtained using (11a). Optimization (29) can also be applied to estimate ψ_m in each OC $\beta \in \{1,\dots,N_{\mathrm{OC}}\}$ by substituting β, $\tilde{\varepsilon}_{R_\alpha \mathrm{tot}}$, and $\tilde{R}'_{\mathrm{ac}_\alpha}$, with α, $\tilde{\varepsilon}_{\psi_\beta \mathrm{tot}}$, and $\tilde{\psi}_{m_\beta}$, respectively. It is worth noting that according to (29), when only two OCs are available, the proposed method evaluates the reliability of the achievable estimation. Instead, when more than two OCs are available, the proposed algorithm selects the best AOC that minimizes the error majorant.

TABLE I
MOTOR DRIVE PARAMETER

Parameter	Motor drive	Unit
Rated power	4.20	kW
Rated speed	80	krpm
Rated Current	7	A
DC link voltage	540	V
Number of pole pairs	2	
R_{DC_0}	0.67	Ω
ψ_{m0}	26.82	mWb
L	1.25	mH
α_{PM0}	-0.035	$\%/^\circ C$
Sampling time (T_s)	25	μs

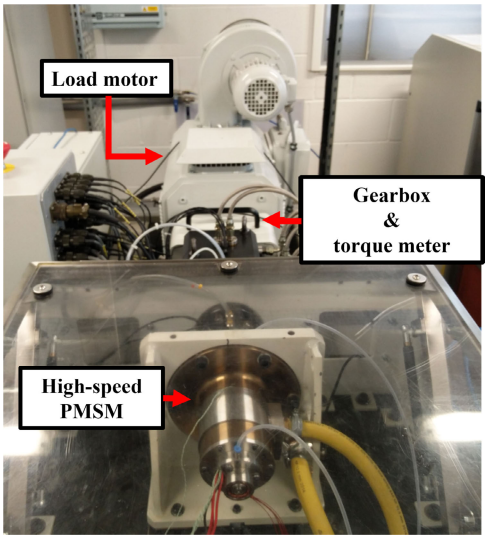

Fig. 3. Experimental setup.

IV. VALIDATION METHODOLOGY

The proposed identification procedure is validated on a challenging case study consisting of a custom high-speed PMSM drive with large parameter variations. The specifications of the motor drive are reported in Table I while the setup is shown in Fig. 3. Note that the reported stator resistance value is obtained using an ohmmeter at the room temperature while the stator inductance and rotor flux linkage are derived with the experimental procedure reported in [32], which matches the finite element analysis presented in [33]. The stator inductance can be considered constant as this particular machine is not affected by magnetic saturation. The high-speed PMSM is connected to a load motor via a gearbox and a torque sensor, and a custom three-phase VSI has been used to supply the motor. The field-oriented control ($i_d = 0$) has been implemented on a Xilinx Zynq7020 SoC custom control platform.

Section V reports the results obtained considering different scenarios derived from a simulation dataset obtained using a MATLAB/Simulink model of this motor drive. The full experimental dataset considered to validate the proposed method is made up of measurements collected during efficiency characterization of this machine [33]. This dataset, $\mathcal{X}$, consists of 20 different steady-states with high temperature, current, and speed variations. In all, 55 OCs are extracted from $\mathcal{X}$ by adopting the procedure described in Section III-A and by setting $\Delta\Theta_r = 1\ ^\circ\mathrm{C}$ and $\Delta\Theta_s = 15\ ^\circ\mathrm{C}$. Fig. 4 reports the

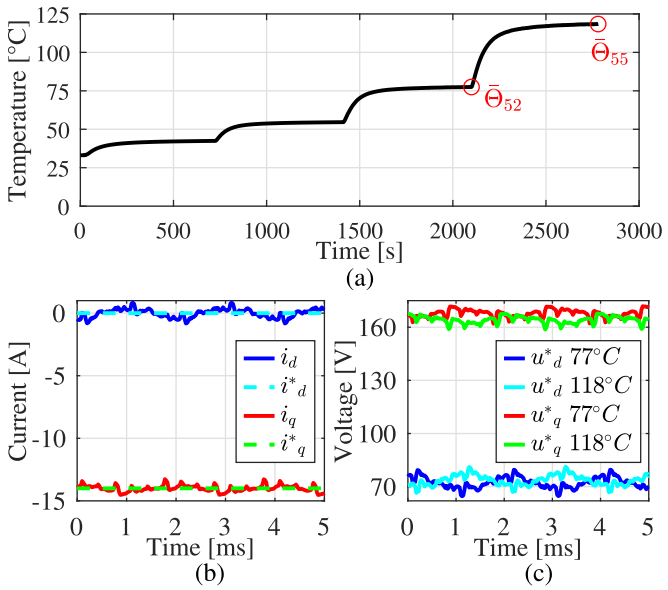

Fig. 4. Measurements during the test at 30 krpm of motor drive 1: (a) temperature, (b) dq-axis actual and reference currents at 77 °C, and (c) dq-axis voltage references at 77 °C and 118 °C.

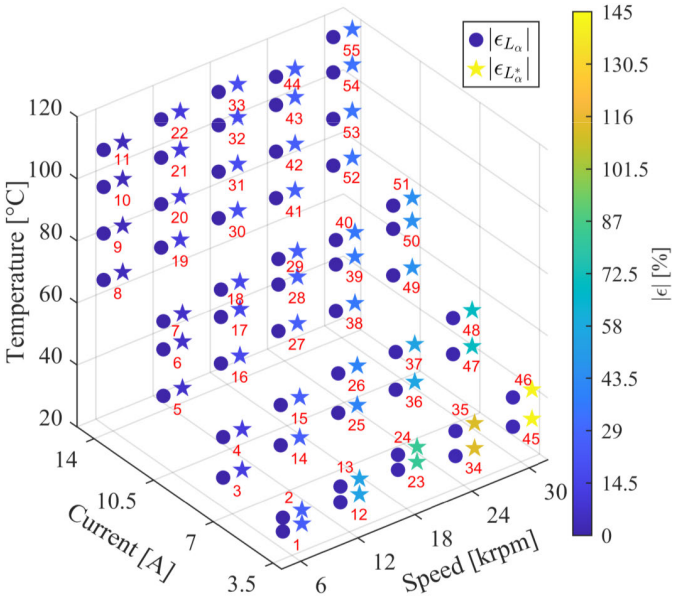

Fig. 5. Estimation error of L.

main variables during the test at 30 krpm. Fig. 4(a) shows the winding temperature. Two temperature points (77 °C and 118 °C) corresponding to OCs 52 and 55 are highlighted with the marker. Note that as shown in Fig. 4, the average value of i_q in these two OCs is the same. Fig. 4(b) reports the measured and reference currents corresponding to OC 52, while Fig. 4(c) shows the voltage references corresponding to OCs 52 and 55. As expected, only the q-axis voltage references are affected by the temperature variation due to the changes in ψ_m and R.

The simulation dataset reproduces the same 55 OCs of the experimental dataset allowing the validation of the proposed method in an extended operating range of the motor. In fact, note that the actual values of L, ψ_m, R, V_{dead}, and dq-axis voltages are difficult to measure in all the experimental OCs. In the simulation model, the parameters' dependence on the OCs is implemented as follows:

$$\begin{aligned} R'_{\text{ac}} &= R_{\text{dc}_0} \frac{\left(R'_{\text{ac}}|_{20}\right) - 1}{\left(1 + \alpha_0 \left(\bar{\Theta}_t - 20\right)\right)^{\gamma+1}} + R_{\text{dc}_0} \\ \psi_m &= \psi_{m0} \left(1 + \alpha_{\text{PM0}} \left(\Theta - 20\right)\right) \end{aligned} \tag{30}$$

where $R'_{\text{ac}}|_{20}$ is a 1-D lookup table containing the experimental ac stator resistance measurements at 20 °C, R_{dc_0} is the experimental measurement value of the dc stator resistance at 20 °C, and $\gamma = 0.75$. Note that the value of β_0 that fits the experimental measurements $R'_{\text{ac}}|_{20}$ is approximately equal to $3.52{\cdot}10^{-7}/\text{Hz}^2$. The inverter parameters ($V_{\text{dead}} = -0.35$ V) are considered constant during the simulations and the inductance which do not significantly depend on the q-axis current in the investigated case study, according to the measurements performed on the real motor. The other parameters required by the proposed procedure are set as follows: $\tilde{\varepsilon}_{u_q} = 0.5$ V, $\tilde{\beta}_0 = 1.27 \cdot 10^{-6}/\text{Hz}^2$ $r_{\text{lim}} = 2$, $\Theta_{\text{lim}} = 20$ °C, $f_{\text{lim}} = 2$, $\varepsilon_{r_1} = 0.9$, $\varepsilon_{r_2} = 1.1$, and $x_R = 0.25$.

V. Simulation Results

A. Identification of L and V_{dead}

This section presents the results of the identification of L and V_{dead} in all the extracted 55 OCs. Fig. 5 reports with the color scale in the current–speed–temperature space the actual estimation absolute percentage error (APE) of L defined as $\epsilon_{L_\alpha} = 100|(\hat{L}_\alpha - L_\alpha)/L_\alpha|$. In the same figure, $\epsilon_{L^*_\alpha}$ represents the APE related to the estimations obtained without compensating the digital delay according to (3). The identification of L using the compensation of the digital delay is highly accurate with a mean APE (MAPE) of 0.51% and a maximum error $\varepsilon_{L_{46}} = 2.75\%$. Also, the standard deviation (SD) of the estimation error is low (0.68%). Instead, as expected, the results obtained without the compensation of the digital delay are affected by large errors which increase with the motor speed.

To demonstrate the stator inductance tracking ability under saturation effects of the proposed algorithm, an additional analysis is reported. The dependence of L on the q-axis current has been introduced in the simulation model to take into account the saturation effect. The upper subfigure in Fig. 6 shows the q-axis current before and after an abrupt load torque variation. Thanks to the R-statistic algorithm, the two different steady-states of i_q can be easily detected and two different OCs can be extracted. In fact, before the load torque change, the R-statistic index (R_{i_q}) is below the critical threshold (R_{crt}) which means that i_q is at the steady-state [16]. The measurements in this time interval constitute the first OC. When i_q arises due to the load torque change, the R-statistic algorithm timely detects the loss of steady-state ($R_{i_q} > R_{\text{crt}}$). The measurements in this time window can therefore be excluded from the dataset used to estimate the parameters. Finally, R_{i_q} quickly approaches the unity when the steady-state is recovered and a new OC is extracted. Note that to correctly extract the OCs, the R-statistic procedure is

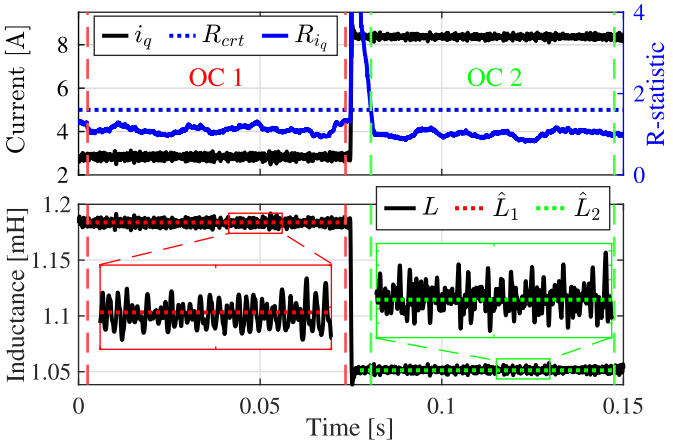

Fig. 6. Estimation of L under saturated conditions.

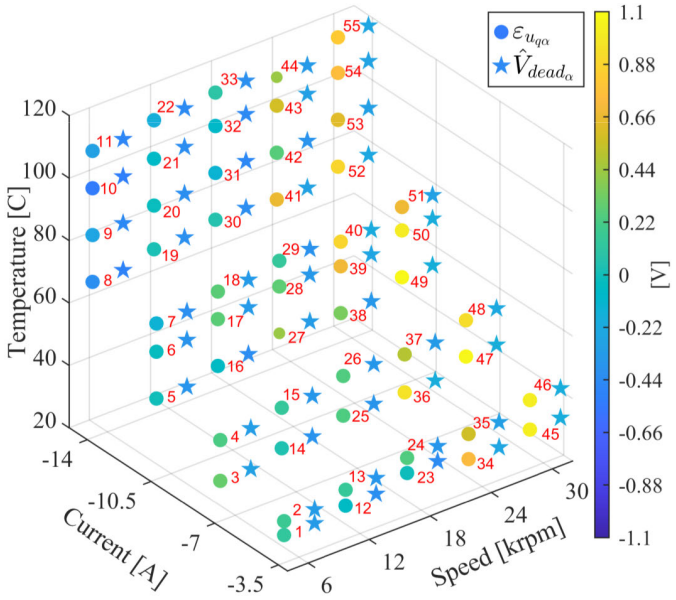

Fig. 7. Voltage error and identified distorted voltage term.

also applied on the rotor speed, as mentioned in Section III-A. In the lower subfigure, the trend of the actual stator inductance is reported along with its estimations in the two extracted OCs. According to the saturation effect, the actual stator inductance decreases with the increase in the current. Albeit its variation, the inductance in the two different OCs is tracked very precisely by the proposed algorithm. The reason behind this is that since from (7) only a single OC is required to estimate L, the accuracy of the proposed algorithm is not affected by inductance variations due to saturation effects. In fact, as i_q is constant within the two OCs, L is also constant. It can be concluded that in the presence of saturation effects, the proposed method can track the inductance variation by estimating the inductance in OCs with different currents.

Fig. 7 reports with the color scale the q-axis voltage error, $\varepsilon_{u_{q\alpha}}$, and $\hat{V}_{\text{dead}_\alpha}$, ($\alpha = 1, \ldots, 55$), in the current–speed–temperature space. $\varepsilon_{u_{q\alpha}}$ has been computed as

$$\varepsilon_{u_{q\alpha}} = \tilde{\bar{u}}_{q_\alpha} + \bar{D}_{q_\alpha} \hat{V}_{\text{dead}_\alpha} - \bar{u}_{q_\alpha}, \quad \alpha = 1, \ldots, 55 \tag{31}$$

where $\bar{u}_{q_\alpha}$ is the average actual q-axis voltage. The mean absolute error (MAE) of $\varepsilon_{u_{q\alpha}}$ is 0.40 V, while the maximum error is $\varepsilon_{u_{q49}} = 1.08$ V. Note that $\varepsilon_{u_{q\alpha}}$ increases as the speed increases since fewer samples are available in a period of $D_d V_{\text{dead}}$. The average value of $\hat{V}_{\text{dead}_\alpha}$ is -0.34 V, which is really close to the actual value, and the SD is 2.5%. Therefore, the proposed method provides accurate estimations of the actual q-axis voltage in a wide range of OCs.

B. Identification of R'_{ac} and ψ_m

This section presents the results of the identification of R'_{ac} and ψ_m considering different scenarios. Fig. 8 shows the results obtained considering the first five steady-states, which correspond to the first 13 OCs shown in Fig. 5. In this figure, $\epsilon_{\%\psi_\alpha}$ and $\epsilon_{\%R_\alpha}$ represent the actual APEs, computed similar to $\epsilon_{\%L_\alpha}$; $\varepsilon_{\%\psi_\alpha} = 100|(\varepsilon_{\psi_\alpha} + \varepsilon_{\psi_M})/\psi_\alpha|$ and $\varepsilon_{\%R_\alpha} = 100|(\varepsilon_{R_\alpha} + \varepsilon_{R_M})/R'_{\text{ac}_\alpha}|$ are the theoretical APEs computed, respectively, using (14) and (16) with the actual values of the parameters and q-axis voltage errors; and $\tilde{\varepsilon}_{\%\psi_\alpha} = 100|(\tilde{\varepsilon}_{\psi_\alpha \text{tot}})/\psi_\alpha|$ and $\tilde{\varepsilon}_{\%R_\alpha} = 100|(\tilde{\varepsilon}_{R_\alpha \text{tot}})/R_\alpha|$ are the minimized absolute percentage values of the error majorants, obtained according to (29). Note that $\varepsilon_{\%\psi_\alpha} \approx \epsilon_{\%\psi_\alpha}$ and $\varepsilon_{\%R_\alpha} \approx \epsilon_{\%R_\alpha}$ in all the OCs. This outcome confirms the validity of the error analysis performed in Section III. In addition, $\tilde{\varepsilon}_{\%\psi_\alpha} > \epsilon_{\%\psi_\alpha}$ and $\tilde{\varepsilon}_{\%R_\alpha} > \epsilon_{\%R_\alpha}$ in all the OCs, confirming the correct definition of the error majorant. Note that in some OCs, the actual and theoretical APEs of R'_{ac} are not shown as in these cases the estimations have been rejected according to (29). Overall, low estimation errors have been obtained even if the results are asymmetric for the two parameters. In fact, R'_{ac} is the most difficult parameter to be identified due to its high dependence on the OCs.

Fig. 9 shows the results obtained considering the same set of OCs but with $\tilde{\varepsilon}_{u_q} = 0$ V, i.e., the voltage error is not considered for the minimization of the error majorant in (29). Note how the estimation accuracy is overall deteriorated for both ψ_m and R'_{ac} and that the error majorant is lower than the actual error in several OCs. It is clear that even if the q-axis voltage error $\varepsilon_{u_{q\alpha}}$ is small, as shown in Fig. 7, it largely affects the estimation accuracy and must be taken into account for the minimization of the error majorant.

Fig. 10 shows a performance analysis of the identification of ψ_m and R'_{ac} considering several scenarios with different numbers of available steady-states. For each scenario s, N_s different trials produced by randomly choosing k_s steady-states among $\mathcal{X}$, with $k_s = 2, \ldots, 10$. Note that since the full dataset contains 20 steady-states, the number of steady-states' combinations without repetition N_{comb_s} when k_s steady-states are considered is given by the following formula:

$$N_{\text{comb}_s} = \frac{20!}{k_s!\,(20 - k_s)!}. \tag{32}$$

In this study, to analyze a congruous number of combinations for each value of k_s, it is set $N_s = N_{\text{comb}_s}/5$. The analysis considers two performance indexes: the MAPE and the number accepted estimations, both averaged over N_s trials. Fig. 10(a) shows the MAPE for both ψ_m and R'_{ac} estimations.

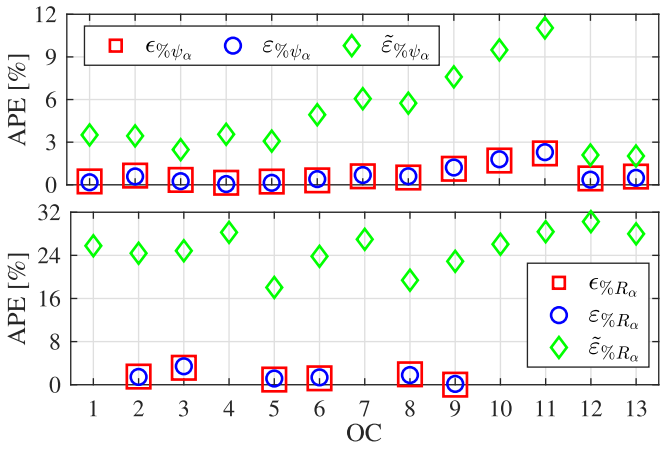

Fig. 8. Results with a set of five steady-states with $\tilde{\varepsilon}_{u_q} = 0.5$ V.

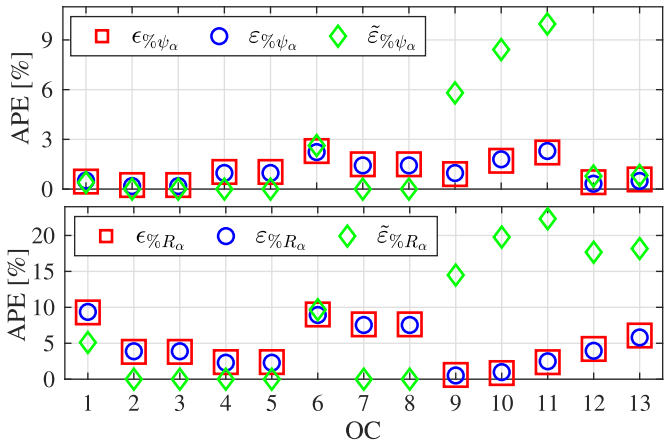

Fig. 9. Results with a set of five steady-states with $\tilde{\varepsilon}_{u_q} = 0$ V.

Despite the challenging case study, the estimation accuracy of ψ_m (blue line) is very high and slightly improves with the increase in the available steady-states. This can be explained considering that the availability of more steady-states increases the chance to further minimize the majorant of the estimation errors. Also, the estimation error of R'_{ac} (red line) is small even if it is significantly greater than the estimation error of ψ_m. Note that in this case, while the average estimation accuracy noticeably improves when going from two to three steady-states, subsequently it slightly deteriorates with the increase in the available steady-states. This can be explained considering the results reported in Fig. 10(b). This figure shows that while the estimations of ψ_m are accepted almost in all the available OCs (the blue line is near to the black line), many estimations of R'_{ac} are rejected. Therefore, with reference to the estimation of R'_{ac}, on average, the increase in the available steady-states may lead to accept estimations previously rejected which can increase the MAPE. It is worth noting that when only two steady-states are available, on average 4 and 0.25 estimations of ψ_m and R'_{ac} are accepted, respectively. This means that with two steady-states, at least an accurate estimation of the rotor flux linkage is guaranteed while the probability to perform reliable estimations of the stator resistance is around 25%. To better demonstrate how

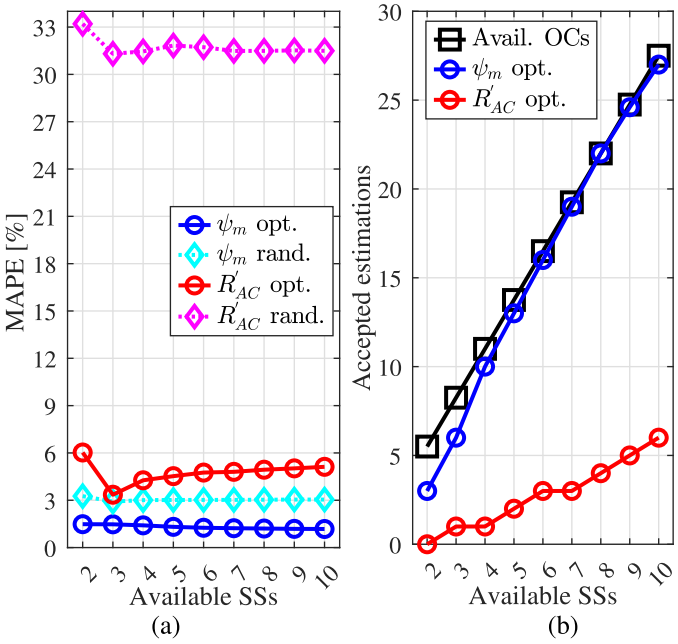

Fig. 10. Identification of ψ_m and R'_{ac} varying the available steady-states: (a) MAPE of the estimation results and (b) average number of accepted estimations compared with the average number of available OCs.

the proposed selection of the AOC improves the accuracy of the parameter estimation, Fig. 10(a) also reports the results obtained by means of a random selection of the AOC (cyan and magenta lines). In particular, for each trial, the AOC is randomly selected among the available OCs that satisfy the condition $r < \varepsilon_{r_1}$ or $r > \varepsilon_{r_2}$, as in (29). This condition prevents to select a value of r close to 1, which would certainly increase the estimation errors according to (14) and (16). Compared with the estimations obtained with the proposed optimization of the error majorant, the random selection of the AOC leads to a lower estimation accuracy of both the parameters. This is particularly clear when looking at the estimation of R'_{ac}. In fact, since this is the parameter most affected by the variation in the OCs, careful selection of the AOC is crucial.

C. Comparison to the State-of-the-Art

In this section, the proposed method is compared with other methods from the literature. Since in the context considered in this article, signal injections and dedicated tests are not possible, two alternative approaches are considered. The first one is based on fixing a parameter to its nominal value while the other parameter is estimated using only one OC [5], [10], [17], [18]. Hereafter, this approach is denoted as fixed parameter (FP) method. When R is fixed to its nominal value R_{dc_0}, the estimation of ψ_m in OC α is provided by

$$\hat{\psi}_{m_\alpha} = \frac{\bar{\tilde{u}}_{q_\alpha} + \bar{D}_{q_\alpha}\hat{V}_{\text{dead}_\alpha} - \bar{i}'_{q_\alpha}R_{\text{dc}_0}}{\bar{\omega}_\alpha}. \tag{33}$$

Note that as in [5], since the current $\bar{i}'_{q_\alpha} = (1 + \alpha_0\Delta\bar{\Theta}_\alpha)\bar{i}_{q_\alpha}$ is used to estimate ψ_m, (33) takes into account the variation in R with the temperature. Instead, when ψ_m is fixed to its

nominal value ψ_{m0}, R'_{ac} can be identified as follows:

$$\hat{R}'_{\text{ac}_\alpha} = \frac{\bar{\tilde{u}}_{q_\alpha} + \bar{D}_{q_\alpha}\hat{V}_{\text{dead}_\alpha} - \bar{\omega}_\alpha\psi_{m0}}{\bar{i}'_{q_\alpha}}. \tag{34}$$

It is worth highlighting that the accuracy of this method does not depend on the quantity of available steady-states as only the data of a single OC are required to estimate the parameters.

The second method is based on a more complex model of the PMSM involving more parameters to explicitly express the dependence of R'_{ac} and ψ_m on the OCs. These parameters are identified by means of the least-squares (LS) method exploiting simultaneously all the available OCs, as in [13] and [26]. The following model derived from (9) and (19) is considered for the generic OC α:

$$\bar{u}'_{q_\alpha} = \bar{i}'_{q_\alpha}R_{\text{dc}_0} + g_\alpha\left(\gamma', \beta'_0\right) + \bar{\omega}_\alpha\psi_{m0} + \bar{\omega}_\alpha\left(\bar{\Theta}_\alpha - 20\right)\alpha'_{\text{PM0}} \tag{35}$$

with $\bar{u}'_{q_\alpha} = \bar{\tilde{u}}_{q_\alpha} + \bar{D}_{q_\alpha}\hat{V}_{\text{dead}_\alpha}$ $\bar{\omega}'_\alpha = \bar{\omega}_\alpha/2\pi$, $\beta'_0 = R_{\text{dc}_0}\beta_0$, $\gamma' = \gamma + 1$, $\alpha'_{\text{PM0}} = \psi_{m0}\alpha_{\text{PM0}}$, and

$$g_\alpha\left(\gamma', \beta'_0\right) = \frac{\bar{i}'_{q_\alpha}\bar{\omega}'^2_\alpha\beta'_0}{\left(1 + \alpha_0\left(\bar{\Theta}_\alpha - 20\right)\right)^{\gamma'}}.$$

This model has five unknown parameters to be identified (R_{dc_0}, β'_0, γ', ψ_{m0}, α'_{PM0}) and is nonlinear on these parameters. This model can be simplified in the affine model shown below

$$\mathbf{y} = \mathbf{X}\boldsymbol{\phi} + \mathbf{b} \tag{36}$$

with

$$\mathbf{y} = \begin{bmatrix} \bar{u}'_{q_1} \\ \vdots \\ \bar{u}'_{q_\alpha} \\ \vdots \\ \bar{u}'_{q_{N_{\text{OC}}}} \end{bmatrix}, \quad \boldsymbol{\phi} = \begin{bmatrix} R_{\text{dc}_0} \\ \gamma' \\ \beta'_0 \\ \psi_{m0} \\ \alpha'_{\text{PM0}} \end{bmatrix}, \quad \mathbf{b} = \begin{bmatrix} b_1 \\ \vdots \\ b_\alpha \\ \vdots \\ b_{N_{\text{OC}}} \end{bmatrix}$$

$$\mathbf{X} = \begin{bmatrix} \bar{i}'_{q_1} & p_1 & q_1 & \bar{\omega}_1 & \bar{\omega}_1\left(\bar{\Theta}_1 - 20\right) \\ \vdots & \vdots & \vdots & \vdots & \vdots \\ \bar{i}'_{q_\alpha} & p_\alpha & q_\alpha & \bar{\omega}_\alpha & \bar{\omega}_\alpha\left(\bar{\Theta}_\alpha - 20\right) \\ \vdots & \vdots & \vdots & \vdots & \vdots \\ \bar{i}'_{q_{N_{\text{OC}}}} & p_{N_{\text{OC}}} & q_{N_{\text{OC}}} & \bar{\omega}_{N_{\text{OC}}} & \bar{\omega}_{N_{\text{OC}}}\left(\bar{\Theta}_{N_{\text{OC}}} - 20\right) \end{bmatrix}$$

where p_α, q_α, and b_α are coefficients obtained from the first-order Taylor approximation of the function $g_\alpha(\gamma', \beta'_0)$ on the point $(\bar{\gamma}', \bar{\beta}'_0)$, with $\bar{\gamma}' = 1.5$ and $\bar{\beta}'_0 = \tilde{\beta}_0/2$, which is chosen according to the considerations reported in Section III-D.

The LS finds the solution $\hat{\boldsymbol{\phi}}$ that minimizes the voltage prediction error on the model (36)

$$\hat{\boldsymbol{\phi}} = \left(\mathbf{X}^\top\mathbf{X}\right)^{-1}\left(\mathbf{X}^\top\mathbf{y} - \mathbf{X}^\top\mathbf{b}\right). \tag{37}$$

The parameters R'_{ac} and ψ_m in OC α are obtained as follows:

$$\hat{R}'_{\text{ac}_\alpha} = \frac{(\mathbf{X})_{\alpha,1:3}\left(\hat{\boldsymbol{\phi}}\right)_{1:3}}{\bar{i}'_{q_\alpha}} + b_\alpha$$

$$\hat{\psi}_{m_\alpha} = \frac{(\mathbf{X})_{\alpha,4:5}\left(\hat{\boldsymbol{\phi}}\right)_{4:5}}{\bar{\omega}_\alpha} \tag{38}$$

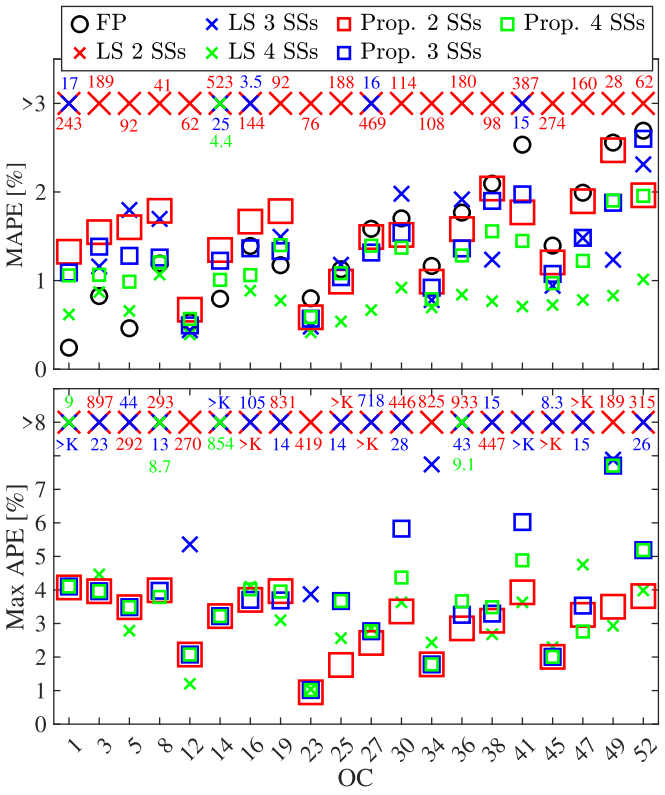

Fig. 11. Estimation errors of ψ_m with different methods and with two, three, and four available steady-states. The numbers at the top of the subfigures denote percentage errors >3% and >8%.

where $(\mathbf{X})_{\alpha,i:j}$ expresses the elements from the ith to jth rows of the αth column of $\mathbf{X}$. To compare these two methods with the one proposed in this article, an analysis considering scenarios with different numbers of available steady-states is reported. The performances are compared over a set of 20 OCs, i.e., the first OCs of each steady-state (see Fig. 5). As in the analysis shown in Fig. 10, for each OC, a number of trials provided by (32) are performed. Fig. 11 shows the MAPE and the maximum APE of the estimation of ψ_m when two, three, and four steady-states are available. The black circles in the upper figure represent the estimations obtained with the FP method. Note that the accuracy decreases with the increase in the motor speed as the variation in R with the frequency is not taken into account by this method. Moreover, also the voltage errors cannot be compensated with the FP method. Therefore, the proposed method outperforms the FP method almost in all the OCs even with few available steady-states. At the top of the two subfigures are reported the estimations with MAPE and maximum APE higher than 3% and 8%, respectively. In these cases, a numeric value is added to specify the errors. Clearly, the LS fails when only two steady-states are available since the number of the OCs is insufficient to correctly estimate $\hat{\boldsymbol{\phi}}$.

Instead, the proposed method provides reliable estimations with low maximum APE. When three steady-states are available, the proposed method is still more accurate than the LS (for most of the OCs, the blue squares are below the blue crosses). Finally, when four steady-states are available, the

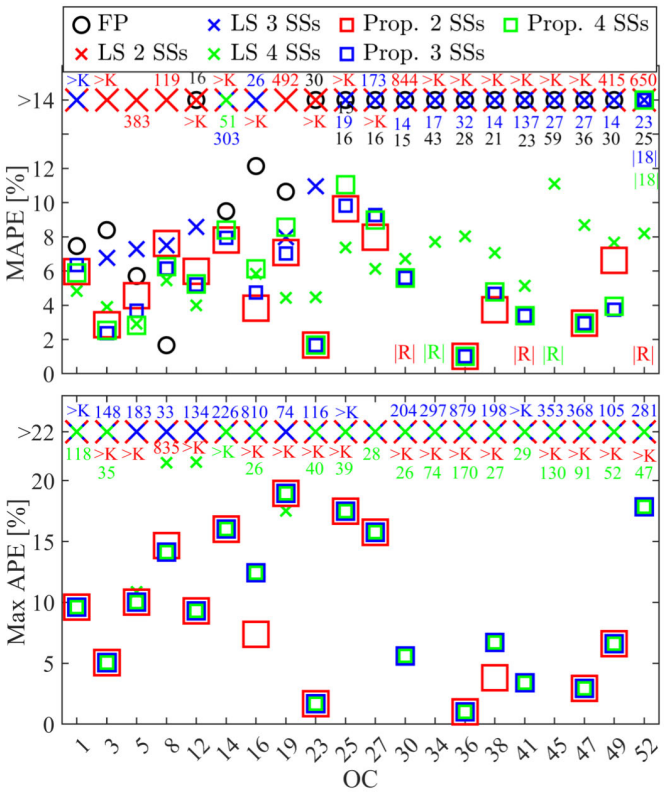

Fig. 12. Estimation errors of R'_{ac} with different methods and with two, three, and four available steady-states. The numbers at the top of the subfigures denote percentage errors $>14\%$ and $>22\%$.

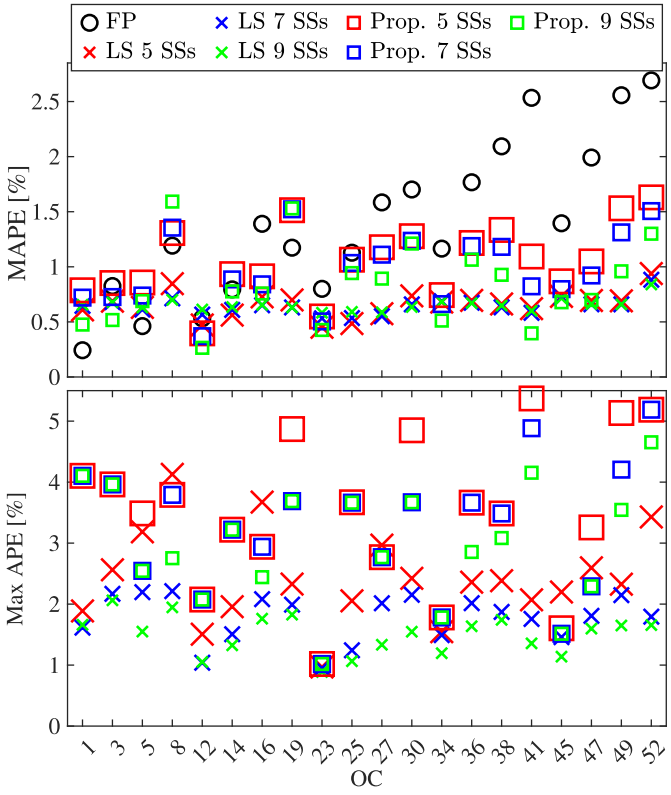

Fig. 13. Estimation errors of ψ_m with different methods and with five, seven, and nine available steady-states.

MAPEs obtained with the LS are lower than those of the proposed method. Instead, the maximum APEs are greater for the LS than for the proposed method in most of the OCs.

Fig. 12 reports the same analysis for R'_{ac}. Also in this case, the FP method is poorly accurate and is outperformed by the proposed method. This is mainly caused by the fact that this method does not take into account the variation in ψ_m with the temperature. In this figure, the symbol $>K$ that appears on the top of the subfigures denotes that the error is greater than 1000%. Moreover, the symbol $|R|$ denotes that the estimation has been rejected by the proposed method. As concerning the MAPE, with the same available steady-states, the LS is on average outperformed by the proposed method in all the cases. Instead, as concerning the maximum APE, the gap between the LS and the proposed method is even bigger. This is mainly due to the fact that the proposed method rejects the estimations affected by a high error majorant.

Fig. 13 shows the results of the estimations of ψ_m when five, seven, and nine steady-states are available. The results obtained with the FP method are the same reported in Fig. 11. As concerning the MAPE, the LS outperforms the proposed method when five or seven steady-states are available, while the performances of the two methods are quite similar when nine steady-states are available. Instead, in all the cases, the maximum APEs obtained with the proposed method are higher if compared with the LS.

Finally, Fig. 14 reports the same analysis for R'_{ac}. Note that although the LS generally achieves lower MAPEs across all the three scenarios on average, the proposed method, on the other hand, exhibits significantly lower maximum APEs. It is worth noting that with the LS method, even when significant parameter estimation errors occur, the voltage prediction errors remain close to zero. Therefore, a criterion to reject estimations affected by high-voltage prediction errors would be ineffective. Instead, the proposed method ensures to limit the maximum estimation error by taking into account the voltage errors and parameter variations.

VI. Experimental Results

This section reports the results obtained with the experimental dataset. Fig. 15 shows the results of the identification of L in all the 55 OCs using the d-axis compensated voltage and the d-axis voltage reference ($\hat{L}^*_\alpha$). The estimations are compared with the measured value. Note that the estimations obtained with the compensated voltage are very accurate, and, as expected, the identified L does not significantly vary with both current and speed. Instead, the estimations obtained with the voltage reference worsen with the increase in the speed, as in the simulation analysis.

Regarding the identification of ψ_m and R'_{ac}, since only measurements of these parameters at room temperature are available, to properly evaluate the estimation accuracy, Fig. 16 shows the results obtained on a reduced subset of OCs, i.e., the OCs at temperature lower than 50 °C. In particular, the results have been obtained considering a scenario with five available steady-states. The available steady-states are randomly chosen among the full dataset, and a number of trials equal to

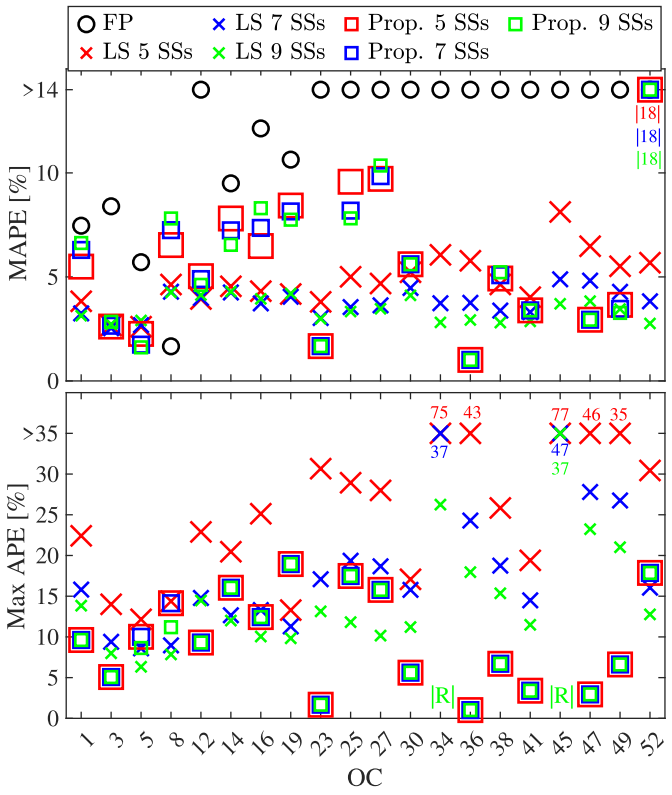

Fig. 14. Estimation errors of R'_{ac} with different methods and with five, seven, and nine available steady-states. The numbers at the top of the subfigures denote percentage errors >14% and >35%.

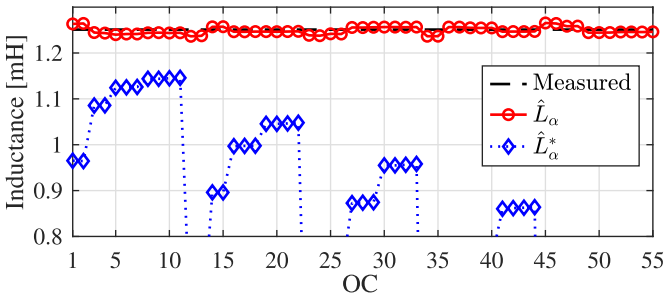

Fig. 15. Estimation of L.

$N_5 = N_{\text{comb}_5}/5$ is evaluated. Since the maximum temperature difference with respect to the room temperature is 30 °C, the variation in the actual ψ_m and R'_{ac} can be neglected. The analysis is performed in three different cases, i.e., when setting $\tilde{\varepsilon}_{u_q} = 0.5$ V, $\tilde{\varepsilon}_{u_q} = 0$ V, and $\tilde{\varepsilon}_{u_q} = 0.5$ V with $\hat{V}_{\text{dead}} = 0$ V. The third case allows to analyze the estimation accuracy when the VSI nonlinearity is not compensated. In particular, the figure shows the average and worst values of the estimations obtained with N_5 trials. As concerns the estimation of ψ_m, the average estimations are very similar in the two first cases, with a high accuracy. However, in some OCs, the worst estimations obtained in the first case are more accurate than in the second one, confirming the importance of considering the voltage error to minimize the error majorant. Note also that the average estimations slightly decrease with the increase in OCs' temperature (see Fig. 5). This aspect highlights that the proposed method can detect slight rotor flux linkage variations with the temperature. Also, the average

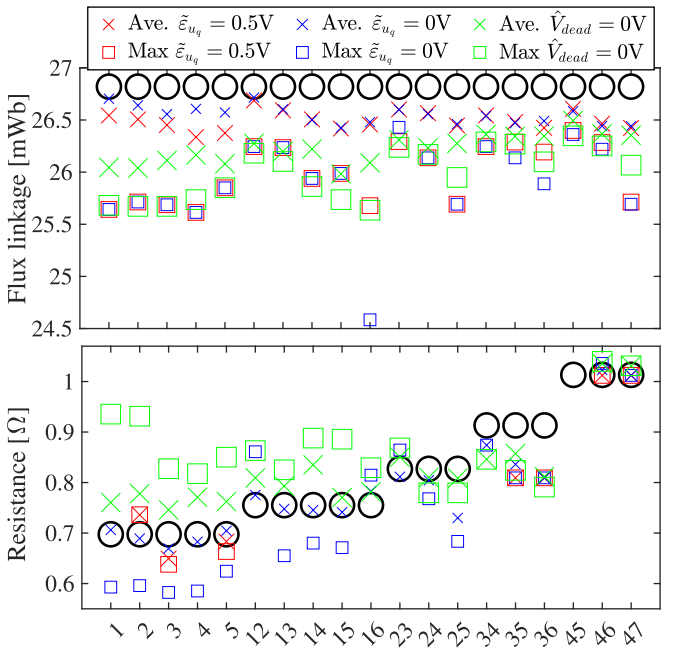

Fig. 16. Estimation of ψ_m and R'_{ac} with five steady-states. The black circles represent measured values.

estimations of R'_{ac} are highly accurate and can precisely track the resistance variations with the speed of the motor. In the first case ($\tilde{\varepsilon}_{u_q} = 0.5$ V), the estimations are accepted only in few OCs, in a similar way to the simulation results shown in Fig. 8. Furthermore, the considerations drawn on the comparison between the average and worst estimations of ψ_m in the two first cases can also be repeated about the estimation of R'_{ac}. Finally, this analysis demonstrates the importance of estimating the distorted voltage. In fact, in most of the OCs the estimation accuracy decreases for both ψ_m and R'_{ac} when the VSI nonlinearity is not compensated.

VII. Conclusion

This article has investigated the possibility of estimating the parameters of an isotropic PMSM only using the measurements commonly available during the regular operation of commercial drives. The rank-deficiency issue, typical of this class of problem, is solved using two different OCs. In particular, by properly selecting these two OCs from the available dataset of measurements, it is possible to minimize the estimation errors due to both parameter variations and voltage errors. The effectiveness of the proposed identification approach has been validated using both the simulation and experimental studies considering several scenarios with different numbers of available speed/load OCs. The key findings of the article are summarized as follows: 1) the accuracy of the estimations of both ψ_m and R improves when the q-axis voltage error component is considered when selecting the optimal OCs required to perform their identification; 2) the accuracy of the estimations improves when more steady-states are available; and 3) the number of identifiable OC increases with the size of the available dataset of measurements. Also, the proposed method has been compared with other methods from the literature. The results clearly show that the proposed

method outperforms the method based on fixing a parameter to its nominal value. In addition, the proposed approach works better than the LS method in scenarios with a limited number of steady-states. Although, on average, the LS technique performs better than the proposed one in scenarios with more than four available steady-states, the estimations of the stator resistance produced by the LS method are impacted by larger maximum errors. Hence, the proposed method is more flexible as it provides accurate estimations even in scenarios with few available steady-states and is more cautionary as it autonomously rejects estimations affected by high errors. These outcomes demonstrate the superiority of the proposed identification method to any application where additional sensor, dedicated tests, and signal injections are not possible. Such feature makes the proposed method highly suitable for condition monitoring of large-scale industrial plants where many electrical machines are operating at the same time.

REFERENCES

[1] X. Wang, S. Lu, W. Huang, Q. Wang, S. Zhang, and M. Xia, "Efficient data reduction at the edge of industrial Internet of Things for PMSM bearing fault diagnosis," *IEEE Trans. Instrum. Meas.*, vol. 70, pp. 1–12, 2021.

[2] A. L. Dias, A. C. Turcato, G. S. Sestito, D. Brandao, and R. Nicoletti, "A cloud-based condition monitoring system for fault detection in rotating machines using PROFINET process data," *Comput. Ind.*, vol. 126, Apr. 2021, Art. no. 103394.

[3] D. Gonzalez-Jimenez, J. del-Olmo, J. Poza, F. Garramiola, and P. Madina, "Data-driven fault diagnosis for electric drives: A review," *Sensors*, vol. 21, no. 12, p. 4024, Jun. 2021.

[4] X. Dai and Z. Gao, "From model, signal to knowledge: A data-driven perspective of fault detection and diagnosis," *IEEE Trans. Ind. Informat.*, vol. 9, no. 4, pp. 2226–2238, Nov. 2013.

[5] K. Liu and Z. Q. Zhu, "Online estimation of the rotor flux linkage and voltage-source inverter nonlinearity in permanent magnet synchronous machine drives," *IEEE Trans. Power Electron.*, vol. 29, no. 1, pp. 418–427, Jan. 2014.

[6] Z.-H. Liu, H.-L. Wei, X.-H. Li, K. Liu, and Q.-C. Zhong, "Global identification of electrical and mechanical parameters in PMSM drive based on dynamic self-learning PSO," *IEEE Trans. Power Electron.*, vol. 33, no. 12, pp. 10858–10871, Dec. 2018.

[7] J. Huo, H. Ji, and P. Yang, "Research on sensorless control system of permanent magnet synchronous motor for CNC machine tool," in *Proc. 40th Chin. Control Conf. (CCC)*, Jul. 2021, pp. 1592–1595.

[8] A. Floris, M. Porru, A. Damiano, and A. Serpi, "Design of a high-speed electric propulsion system for electric vehicles," in *Proc. AEIT Int. Conf. Electr. Electron. Technol. Automot. (AEIT AUTOMOTIVE)*, Nov. 2020, pp. 1–6.

[9] A. Floris, A. Damiano, and A. Serpi, "Design of high-speed/high-power PM synchronous machines for an adiabatic compressed air storage system," in *Proc. Int. Conf. Electr. Mach. (ICEM)*, Sep. 2022, pp. 935–941.

[10] Z. Q. Zhu, D. Liang, and K. Liu, "Online parameter estimation for permanent magnet synchronous machines: An overview," *IEEE Access*, vol. 9, pp. 59059–59084, 2021.

[11] O. Sandre-Hernandez, R. Morales-Caporal, J. Rangel-Magdaleno, H. Peregrina-Barreto, and J. N. Hernandez-Perez, "Parameter identification of PMSMs using experimental measurements and a PSO algorithm," *IEEE Trans. Instrum. Meas.*, vol. 64, no. 8, pp. 2146–2154, Aug. 2015.

[12] C. Candelo-Zuluaga, J.-R. Riba, and A. Garcia, "PMSM parameter estimation for sensorless FOC based on differential power factor," *IEEE Trans. Instrum. Meas.*, vol. 70, pp. 1–12, 2021.

[13] C. Lai, G. Feng, Z. Li, and N. C. Kar, "Computation-efficient decoupled multiparameter estimation of PMSMs from massive redundant measurements," *IEEE Trans. Power Electron.*, vol. 35, no. 10, pp. 10729–10740, Oct. 2020.

[14] K. Liu and Z. Q. Zhu, "Position offset-based parameter estimation for permanent magnet synchronous machines under variable speed control," *IEEE Trans. Power Electron.*, vol. 30, no. 6, pp. 3438–3446, Jun. 2015.

[15] M. Zhou, L. Jiang, and C. Wang, "Real-time multiparameter identification of a salient-pole PMSM based on two steady states," *Energies*, vol. 13, no. 22, p. 6109, Nov. 2020.

[16] E. Brescia, D. Costantino, F. Marzo, P. R. Massenio, G. L. Cascella, and D. Naso, "Automated multistep parameter identification of SPMSMs in large-scale applications using cloud computing resources," *Sensors*, vol. 21, no. 14, p. 4699, Jul. 2021.

[17] T. Boileau, N. Leboeuf, B. Nahid-Mobarakeh, and F. Meibody-Tabar, "Online identification of PMSM parameters: Parameter identifiability and estimator comparative study," *IEEE Trans. Ind. Appl.*, vol. 47, no. 4, pp. 1944–1957, Jul. 2011.

[18] M. A. Hamida, J. De Leon, A. Glumineau, and R. Boisliveau, "An adaptive interconnected observer for sensorless control of PM synchronous motors with online parameter identification," *IEEE Trans. Ind. Electron.*, vol. 60, no. 2, pp. 739–748, Feb. 2013.

[19] O. C. Kivanc and S. B. Ozturk, "Sensorless PMSM drive based on stator feedforward voltage estimation improved with MRAS multiparameter estimation," *IEEE/ASME Trans. Mechatronics*, vol. 23, no. 3, pp. 1326–1337, Jun. 2018.

[20] K. Liu and Z. Q. Zhu, "Position-offset-based parameter estimation using the Adaline NN for condition monitoring of permanent-magnet synchronous machines," *IEEE Trans. Ind. Electron.*, vol. 62, no. 4, pp. 2372–2383, Apr. 2015.

[21] K. Liu, Q. Zhang, J. Chen, Z. Q. Zhu, and J. Zhang, "Online multiparameter estimation of nonsalient-pole PM synchronous machines with temperature variation tracking," *IEEE Trans. Ind. Electron.*, vol. 58, no. 5, pp. 1776–1788, May 2011.

[22] K. Liu and Z. Q. Zhu, "Quantum genetic algorithm-based parameter estimation of PMSM under variable speed control accounting for system identifiability and VSI nonlinearity," *IEEE Trans. Ind. Electron.*, vol. 62, no. 4, pp. 2363–2371, Apr. 2015.

[23] K. Liu, Z. Q. Zhu, Q. Zhang, and J. Zhang, "Influence of nonideal voltage measurement on parameter estimation in permanent-magnet synchronous machines," *IEEE Trans. Ind. Electron.*, vol. 59, no. 6, pp. 2438–2447, Jun. 2012.

[24] Z.-H. Liu, H.-L. Wei, Q.-C. Zhong, K. Liu, and X.-H. Li, "GPU implementation of DPSO-RE algorithm for parameters identification of surface PMSM considering VSI nonlinearity," *IEEE J. Emerg. Sel. Topics Power Electron.*, vol. 5, no. 3, pp. 1334–1345, Sep. 2017.

[25] C. Lai, G. Feng, K. Mukherjee, V. Loukanov, and N. C. Kar, "Torque ripple minimization for interior PMSM with consideration of magnetic saturation incorporating online parameter identification," *IEEE Trans. Magn.*, vol. 53, no. 6, pp. 1–4, Jun. 2017.

[26] G. Feng, C. Lai, X. Tan, W. Peng, and N. C. Kar, "Multi-parameter estimation of PMSM using differential model with core loss compensation," *IEEE Trans. Transport. Electrific.*, vol. 8, no. 1, pp. 1105–1115, Mar. 2022.

[27] R. Wrobel, D. E. Salt, A. Griffo, N. Simpson, and P. H. Mellor, "Derivation and scaling of AC copper loss in thermal modeling of electrical machines," *IEEE Trans. Ind. Electron.*, vol. 61, no. 8, pp. 4412–4420, Aug. 2014.

[28] Q. Wang, G. Wang, S. Liu, G. Zhang, and D. Xu, "An inverter-nonlinearity-immune offline inductance identification method for PMSM drives based on equivalent impedance model," *IEEE Trans. Power Electron.*, vol. 37, no. 6, pp. 7100–7112, Jun. 2022.

[29] D. Fernandez et al., "Permanent magnet temperature estimation in PM synchronous motors using low cost hall effect sensors," in *Proc. IEEE Energy Convers. Congr. Expo. (ECCE)*, Sep. 2016, pp. 1–8.

[30] S. Xiao and A. Griffo, "Online thermal parameter identification for permanent magnet synchronous machines," *IET Electr. Power Appl.*, vol. 14, no. 12, pp. 2340–2347, Dec. 2020.

[31] R. Wrobel, A. Mlot, and P. H. Mellor, "Contribution of end-winding proximity losses to temperature variation in electromagnetic devices," *IEEE Trans. Ind. Electron.*, vol. 59, no. 2, pp. 848–857, Feb. 2012.

[32] E. Armando, R. I. Bojoi, P. Guglielmi, G. Pellegrino, and M. Pastorelli, "Experimental identification of the magnetic model of synchronous machines," *IEEE Trans. Ind. Appl.*, vol. 49, no. 5, pp. 2116–2125, Sep. 2013.

[33] F. Savi et al., "High-speed electric drives: A step towards system design," *IEEE Open J. Ind. Electron. Soc.*, vol. 1, pp. 10–21, 2020.

Open Access funding provided by 'Politecnico di Bari' within the CRUI CARE Agreement